Journal of Hazardous Materials 424 (2022) 127415

Contents lists available at ScienceDirect

Journal of Hazardous Materials

journal homepage: www.elsevier.com/locate/jhazmat

Heterogeneous photo-Fenton degradation toward sulfonamide matrix over magnetic Fe_3S_4 derived from MIL-100(Fe)

Jing Hang [a], Xiao-Hong Yi [a], Chong-Chen Wang [a,*], Huifen Fu [a], Peng Wang [a], Yijiang Zhao [b,*]

[a] Beijing Key Laboratory of Functional Materials for Building Structure and Environment Remediation/Beijing Energy Conservation & Sustainable Urban and Rural Development Provincial and Ministry Co-construction Collaboration Innovation Center, Beijing University of Civil Engineering and Architecture, Beijing 100044, PR China
[b] School of Chemistry and Chemical Engineering, Huaiyin Normal University, Jiangsu Engineering Laboratory for Environment Functional Materials, No.111 West Changjiang Road, Huaian 223300, Jiangsu Province, PR China

ARTICLE INFO

Editor: Dr. Navid B Saleh

Keywords:
Fe_3S_4
MIL-100(Fe)
Photo-Fenton
Oxidation
Sulfonamide antibiotics

ABSTRACT

Magnetic Fe_3S_4 was facilely derived from MIL-100(Fe) as the precursor and thioacetamide (TAA) as the sulfur source under hydrothermal condition. The as-prepared Fe_3S_4 was adopted as catalyst to promote the photo-Fenton process, in which sulfamethoxazole (SMX) was used as representative pollutant sample to test the oxidative degradation performance of Fe_3S_4. The results showed that Fe_3S_4 exhibited excellent photo-Fenton-like oxidation decomposition performances toward sulfamethoxazole (SMX) under both UV and visible light. A possible degradation mechanism over Fe_3S_4 in the photo-Fenton reaction is put forward based on quenching experiments and electron spin resonance (ESR). About 41% total organic carbon (TOC) removal efficiency of sulfamethoxazole (SMX) over the as-prepared Fe_3S_4 can be accomplished within 40 min. As well, different sulfonamide antibiotics (SAs) like sulfamethoxazole (SMX), sulfisoxazole (SIM) and sulfadiazine (SDZ) were selected to further investigate the oxidative degradation activity of Fe_3S_4 in this photo-Fenton-like reaction system, in which the possible degradation pathways of SMX, SIM and SDZ were put forward based on UHPLC-MS analysis. This work provided a new strategy to prepare magnetic Fe_3S_4 as catalyst for advanced oxidation process, which can be easily separated from the treated water samples to accomplish facile recovery and recyclability.

1. Introduction

Antibiotics are widely used in the prevention and treatment of infections in humans and livestock, which have attracted worldwide attentions in recent years due to their harmful effects on humans and animal organisms even at low concentrations (Chen et al., 2018; Jiang et al., 2020). Sulfonamide antibiotics (SAs), as the first synthetic class of broad-spectrum antibiotics to be used in clinical practice, are widely used until now (Scheme 1). Sulfamethoxazole (SMX) and sulfisoxazole (SIM) are commonly used as human antibiotics (Du et al., 2018b), while sulfadiazine (SDZ) is commonly used as veterinary antibiotics. SAs can be discharged into water bodies through a variety of pathways, resulting in SAs concentrations in wastewater typically in the range between ng/L and μg/L.

Up to now, advanced oxidation processes (AOPs) based on the reactive oxygen species (ROS) like ·OH, $\cdot O_2^-$ and $^1O_2$ rather than the conventional wastewater treatments, have been extensively adopted as an effective and economic technologies for the treatment of emerging and toxic organic pollutants in wastewater (Li et al., 2021). In fact, the photo-Fenton reaction especially the heterogeneous photo-Fenton reaction (Shi et al., 2016; Zhou et al., 2020), has attracted increasing interest in water treatment due to its superior efficiency, low cost and good reusability (Carra et al., 2014; Villegas- Guzman et al., 2017). Various Fe-based catalysts like α-Fe_2O_3@g-C_3N_4 (Guo et al., 2018), TiO_2/Fe_2TiO_5/Fe_2O_3 (Deng et al., 2017), Fe_3O_4@MIL-100(Fe) (He et al., 2021) and MIL-53(Fe) (Ai et al., 2014) have been used to activate the photo-Fenton process for degrading different toxic organic pollutants. However, the difficulty of separating and recycling the photo-Fenton catalysts from the reaction system for recycle and reuse is becoming a serious drawback, which hinders their further practical applications.

Greigite (Fe_3S_4) is a sulfur spinel of iron with similar crystal structure to that of magnetite ($Fe^{2+}Fe^{3+}{}_2S_4$) (Clarizia et al., 2017). It is usually an authigenic ferromagnetic mineral that forms sub-stable precursors to pyrite during the reduction of early diagenetic sedimentary sulfates in

* Corresponding authors.
E-mail addresses: wangchongchen@bucea.edu.cn, chongchenwang@126.com (C.-C. Wang), cyjzhao@126.com (Y. Zhao).

https://doi.org/10.1016/j.jhazmat.2021.127415
Received 1 August 2021; Received in revised form 12 September 2021; Accepted 30 September 2021
Available online 5 October 2021
0304-3894/© 2021 Elsevier B.V. All rights reserved.

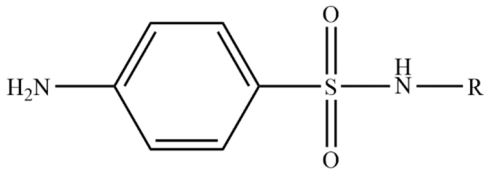

Scheme 1. The structure illustration of sulfonamide antibiotics.

anoxic depositional environments. It also plays an integral role in the global elemental cycle (Roberts et al., 1996; Shi et al., 2020). Due to its ferromagnetic and reducing properties, Fe_3S_4 has been widely used in ion batteries (Li et al., 2017), CO_2 catalytic reduction (Roldan and Leeuw, 2015), heavy metal removal (Liu et al., 2019; Yang et al., 2020), organic arsenic reduction (Liu et al., 2017), N_2 fixation (Zhao et al., 2018), electromagnetic wave absorption (Wu et al., 2020), and biomedical applications (Liu et al., 2020). At the same time, the abundant reduction sites on the surface of Fe_3S_4 can activate H_2O_2 to produce active species for the organic pollutants degradation (Shi et al., 2020). Fe_3S_4 is an outstanding narrow band gap ferromagnetic semiconductor that can be excited by the solar spectrum from the ultraviolet to the infrared (Yang et al., 2017). Electrons in the valence band (VB) of Fe_3S_4 are excited in the conduction band (CB) by light irradiation and then transferred to the surface, in which the photogenerated electrons can reduce the surface Fe(III) to the active Fe(II) in the conduction band. Also, activated H_2O_2 can inhibit the over-oxidation of surface Fe(II) and sulfur. From these points, the advanced oxidation processes achieved over Fe_3S_4 as catalyst might be vast potential for future development.

Metal-organic frameworks (MOFs) constructed from metal nodes and organic ligands are widely investigated in CO_2 reduction (Li et al., 2018), water splitting (Luo et al., 2019), organic pollutants degradation (Zhang et al., 2021), adsorption (Jiang et al., 2019), catalysis (Li et al., 2021) and sensing (Campbell and Dincă, 2017) due to their ultrahigh surface area, structural diversity and tailorability and abundant active sites (Jiao et al., 2018; Wang et al., 2022). Up to now, MOFs were often used as precursors to prepare different functional derivatives like metal sulfides, metal oxides and porous carbon due to that the MOF-derivatives can retain the merits of their MOFs precursors (Fang et al., 2020; Li et al., 2021a, 2021b; Wang et al., 2022; Zhang et al., 2021).

Within this paper, Fe_3S_4 derived from MIL-100(Fe) was applied to accomplish the photo-Fenton degradation toward three sulfonamide antibiotics SMX, SIM and SDZ. The degradation mechanism was confirmed by multiple types of characterization techniques such as radical quenching experiments, electrochemical analysis and ESR tests. The degradation pathways of SMX, SIM and SDZ were identified based on UHPLC-MS analysis. It was expected that this work will provide a new strategy to recovery catalysts in practical wastewater treatment.

2. Experimental

The chemicals, the characterization instruments were described in the Supplementary Information (SI).

2.1. Synthesis of MIL-100(Fe) precursor

MIL-100(Fe) was produced following to the previous literature with slight modification (Xu et al., 2017). Detailly, $FeCl_3{\cdot}6H_2O$ (54.04 mg) and 1,3,5-Benzenetricarboxylic acid (28.16 mg) were dissolved in ethylone glycol (5.0 mL) and dimethylformamide (DMF, 5.0 mL), respectively. The above-mentioned solutions were transferred into the Teflon-lined autoclave to be heated at 393 K for 1 d. The as-obtained MIL-100(Fe) crystals were collected, which were washed in turn with deionized water and ethanol for 3 times.

2.2. Synthesis of magnetic Fe_3S_4

0.1 g as-prepared MIL-100(Fe) and 0.4 g thioacetamide (TAA) were suspended in 15.0 mL absolute ethanol. After ultrasound treatment for 20.0 min, the suspension was sealed in the Teflon-lined autoclave to conduct solvothermal reaction at 120 °C for 12 h. After cooling down to room temperature, the black precipitates were collected by centrifugation with 8000 r/min for 3 min and washed with ultra-pure water and ethanol for three times, respectively. The Fe_3S_4 was obtained by drying at 60 °C overnight.

2.3. Photo-Fenton experiment

15.0 mg Fe_3S_4 was dispersed in 50.0 mL SMX, SIM or SDZ aqueous solution with the initial concentration of 5 mg/L (pH = 5.0) under the ultrasonication. The temperature of reaction solution during the photo-Fenton experiment was maintained at 25 ± 0.3 °C. The pH values of the solutions were adjusted by H_2SO_4 or NaOH solutions with suitable concentrations. After being stirred in dark for 30 min to achieve adsorption-desorption equilibrium, 10 μL 30% H_2O_2 solution (the H_2O_2/SMX molar ratio being 100) was added to the suspension under visible light irradiation (350 mW low power LED light, PCX50C, Beijing Perfectlight Technology Co., Ltd.). At a set interval, 1.0 mL solution was taken out and filtrated with a 0.22 μm nylon filter to determine the residual SMX concentration, in which 0.01 mL of isopropanol was added to quench the reaction. In UV Fenton system, the UV light source (λ = 369 nm) was supplied by a 10 W LED ultraviolet lamp (PCX50B, Beijing Perfectlight Technology Co., Ltd.), while the experiment is identical to the photo-Fenton process.

3. Results and discussions

3.1. Characterizations

The characteristic powder X-ray diffraction (PXRD) patterns of the as-prepared precursor MIL-100(Fe) matched well with those reported in the previous reference (Xu et al., 2017) and the patterns simulated from the single crystal data (cif file of CCDC 640536) (Fig. 1a). As well, the scanning electron microscopy (SEM) observations (Fig. 2a) revealed that the as-synthesized MIL-100(Fe) displayed as highly uniform spheres with the particle size ranging from 200 to 400 nm (Wang et al., 2021). The above characterizations confirmed the successful preparation of the MIL-100(Fe).

After solvothermal treatment with thioacetamide (TAA), the as-obtained precipitates were affirmed as cubic greigite Fe_3S_4 via PXRD, SEM, TEM and HRTEM. It can be found from PXRD patterns that all the diffraction peaks were fully consistent with Fe_3S_4 (JCPDS 16-0713), in which the broad and the sharp PXRD diffraction peaks at $2\theta = 15.5°$, 25.4°, 30.0°, 36.3°, 44.9°, 47.8° and 52.4° can be ascribed to the (1 1 1), (2 2 0), (3 1 1), (4 0 0), (4 2 2), (5 1 1) and (4 4 0) facets of Fe_3S_4 (Yang et al., 2020). The SEM and TEM observations revealed that the as-prepared Fe_3S_4 displayed as uniform nanospheres (Fig. 2b–d), which displayed smaller size (300–500 nm) than that obtained via the template-free method from Luo et al., 2019. The HRTEM micrographs of Fe_3S_4 (Fig. 2e) showed that the fringe spacings of 0.247 nm could be assigned to the (4 0 0) crystalline facet of Fe_3S_4 (JCPDS 16–0713). As exhibited in SAED pattern (Fig. 2f), the diffraction rings of (4 0 0) and (5 1 1) can conveniently be indexed to Fe_3S_4 crystal (Zheng et al., 2014). Additionally, the EDS-mapping was applied to detect the elements distribution of the Fe_3S_4, in which the targeted elements (Fe, S and O) were uniformly distributed over Fe_3S_4 (Fig. S2).

The magnetic hysteresis curve of as-prepared Fe_3S_4 shown in Fig. 1b demonstrated that its saturation magnetization value is 36.3 emu/g (Liu et al., 2017; Yang et al., 2020), indicating that the obtained Fe_3S_4 could be readily collected by the magnetic force. As shown in the inset picture of Fig. 1b, the as-prepared Fe_3S_4 sample could be collected from the

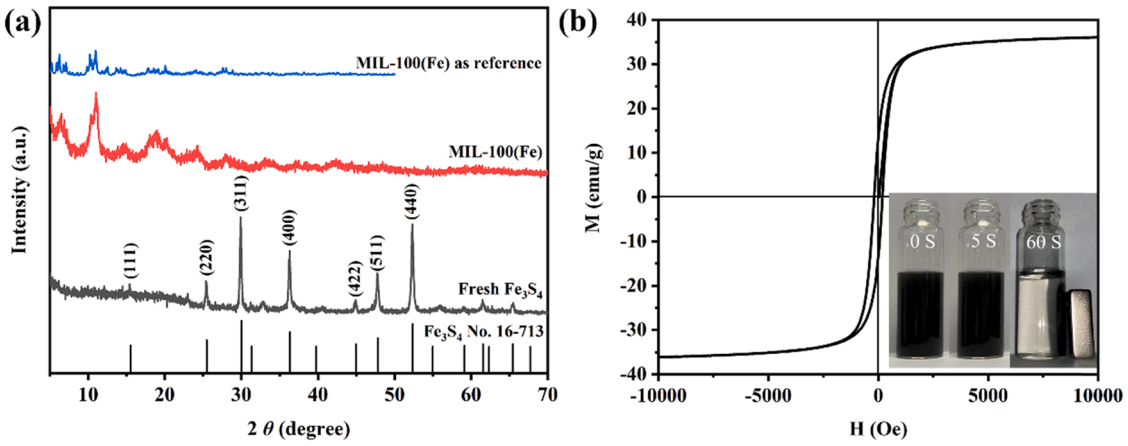

Fig. 1. (a) XRD patterns of as-synthesized materials. (b) Magnetization hysteresis curve of as-prepared Fe_3S_4.

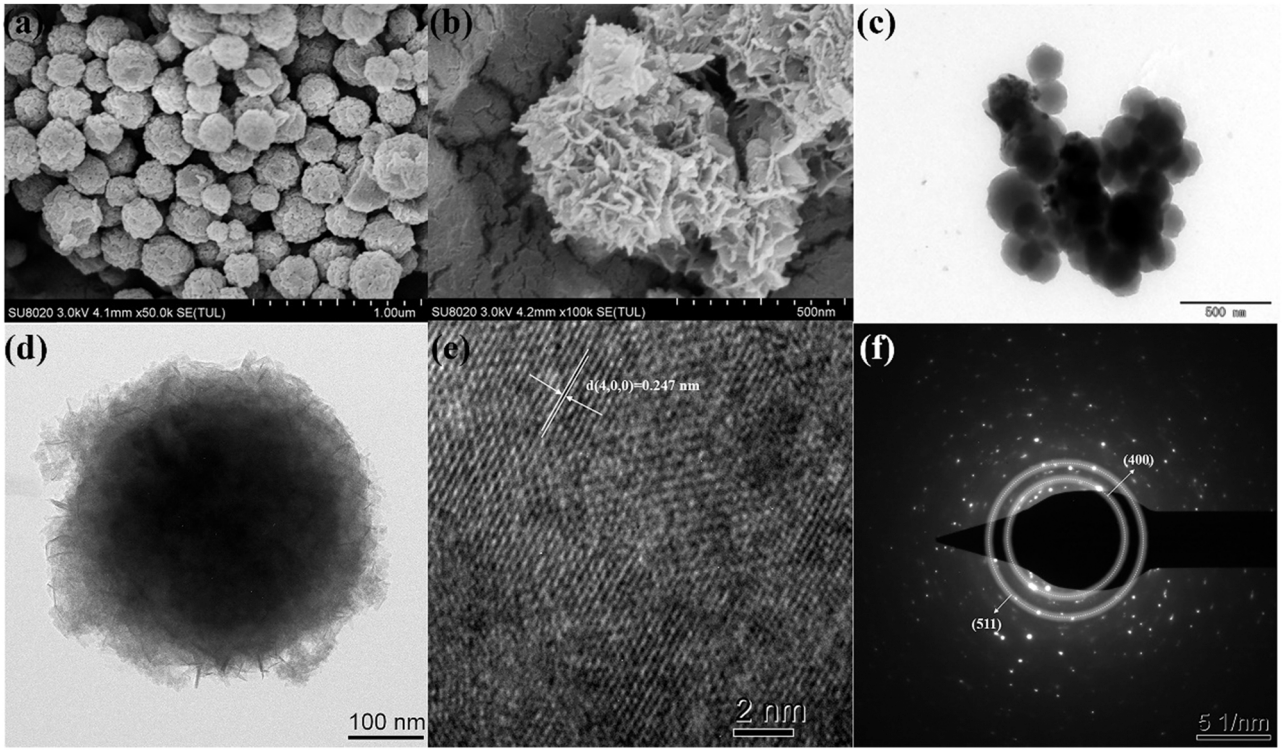

Fig. 2. SEM images of (a) MIL-100(Fe), (b) Fe_3S_4. TEM images of (c) Fe_3S_4. (d–e) HRTEM micrographs and (f) SAED image of Fe_3S_4.

suspension within 60 s with an external magnet.

The UV–vis diffuse reflectance spectra (UV–vis DRS) of the as-prepared Fe_3S_4 (Fig. S1) illustrated that it exhibits strong absorption in both UV–visible and even near-infrared regions, implying Fe_3S_4 can be excited by large range of light (Yang et al., 2017).

3.2. Photo-Fenton activity of Fe_3S_4 derived from MIL-100(Fe)

3.2.1. Heterogeneous Fenton-like reaction performance of Fe_3S_4

The sulfamethoxazole (SMX), as one of the common PPCPs, was selected as organic model to test the photo-Fenton-like degradation performance of Fe_3S_4 as heterogeneous catalyst (Fig. 3a). With the presence of H_2O_2 and low power LED visible light, 100% SMX with initial concentration being 5 mg/L could be degraded over the as-prepared Fe_3S_4 as catalyst within 10 min (pH being 5.0). The Fe_3S_4 had the best SMX degradation activity under UV light irradiation, in which the degradation efficiency was 100% within 5 min. Only 79.1% SMX was decomposed with the presence of Fe_3S_4 and H_2O_2 (heterogeneous Fenton-like process). Also, the series control experiments results revealed that 9.1%, 10.4% and 11.5% SMX could be removed in the Fe_3S_4 system (adsorption process), LED visible light/H_2O_2 system (photo activated H_2O_2 process), and Fe_3S_4/LED visible light (photocatalysis process). It was observed that under the identical conditions, MIL-100 (Fe) demonstrated inferior photo-Fenton SMX degradation performance (17.3%), possibly due to the rapid recombination of the photo-generated carriers (Ahmad et al., 2019). All the above-mentioned results implied that the effective SMX degradation can be contributed to the heterogeneous photo (visible light or UV light)-Fenton-like advanced oxidation process over Fe_3S_4 catalyst.

3.2.2. Influence of initial pH value

It is well known that the solution pH plays a controlling role on the

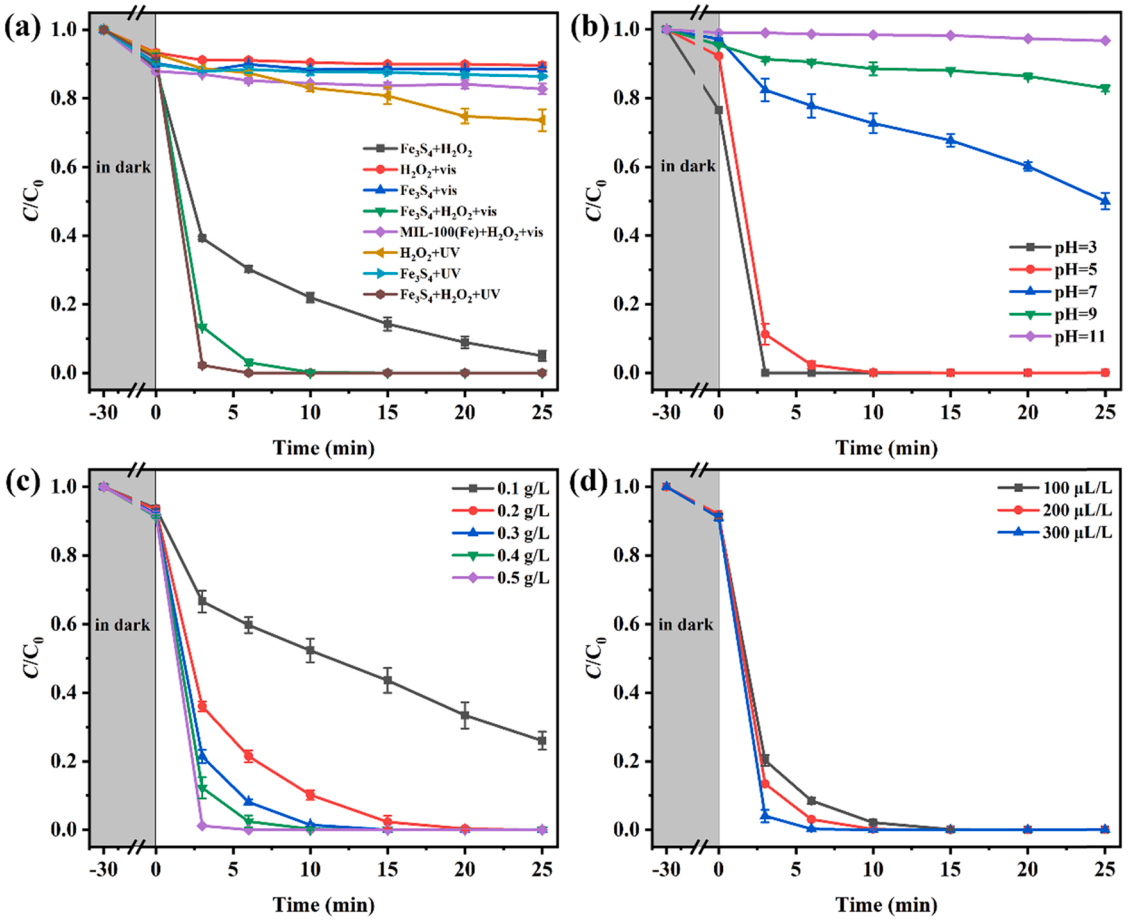

Fig. 3. (a) Photo-Fenton SMX degradation efficiencies in different system. Effect of (b) initial pH, (c) catalyst dosage, and (d) H_2O_2 concentration on the SMX removal efficiencies under visible light irradiation. Reaction conditions: Fe_3S_4 dosage = 0.3 g/L (for a, b, and d), SMX concentration = 5 mg/L, initial pH = 5 (unadjusted, for a, c, and d), H_2O_2 concentration = 200 μL/L (for a–c).

performance of the Fenton-like process in the pollutants removal (Wu et al., 2020) due to its influences the catalytic activity, the existing forms of organic pollutants, the dominant iron species, and the stability of H_2O_2 (Xu and Wang, 2011). The influence of solution pH values on the SMX degradation in the Fe_3S_4/H_2O_2 oxidation process was evaluated at different pH values of 3.0, 5.0, 7.0, 9.0 and 11.0. The results (Fig. 3b) displayed that 100% SMX decomposition can be achieved within 3.0 min at pH being 3.0, implying the acidic conditions can facilitate the formation of the hydroxyl radicals for attacking the SMX pollutants (Daud and Hameed, 2010; Kallel et al., 2009; Xu and Wang, 2011). It was found that 100% SMX can be degraded within 10.0 min at pH being 5.0. In our work, pH being 5.0 was selected for subsequent experiments considering the stability of Fe_3S_4 (Shi et al., 2020) and the real wastewater condition (Clarizia et al., 2017).

3.2.3. *The influence of the catalyst dosage and H_2O_2 concentration*

When the Fe_3S_4 dosage increased from 0.1 g/L to 0.5 g/L (Fig. 3c), the oxidative degradation toward SMX was gradually enhanced, which was attributed to the increase in the active sites of Fe_3S_4 for H_2O_2 decomposition to produce more ROSs like ·OH radicals (Ramirez et al., 2007; Xu and Wang, 2011). Furthermore, the SMX degradation efficiency almost reached 100% within 10 min when the Fe_3S_4 catalyst dosage ranged from 0.3 to 0.5 g/L. From this point, the Fe_3S_4 dosage was selected as 0.3 g/L in the follow-up experiments.

The SMX degradation efficiency increased with the increasing H_2O_2/SMX molar ratio from 50:1 to 150:1 (Fig. 3d), due to that the increasing H_2O_2 could yield more ·OH radicals and further inhibit the quick electron-hole recombination over the Fe_3S_4 during SMX degradation process (Ai et al., 2014). Some counterpart photo-Fenton systems were selected to calculate the H_2O_2/SMX molar ratios (Table S1), in which the as-prepared Fe_3S_4 as catalyst displayed good performance in the view of H_2O_2/organics molar ratio.

3.2.4. *Reusability of catalyst*

The recyclability of Fe_3S_4 was investigated by successive reusability tests (Fig. 4a). The Fe_3S_4 catalyst was regenerated with the aid of the rubidium magnet without any further treatment. After ten cycles of reuse, the SMX degradation efficiencies were maintained at 95.1% in the Fe_3S_4 activated photo-Fenton-like reaction system. It was clearly demonstrated that the Fe_3S_4 exhibited a relatively high recyclability. The leached iron ions concentration was remained between 0.45 mg/L and 0.84 mg/L after each cycle (Fig. 4b), which satisfied the integrated discharge standard of water pollutants (2 mg/L) set by the Beijing local standard (DB11/307-2013). To investigate the role of the homogeneous Fenton resulted from the leaching Fe from Fe_3S_4, $FeCl_2$ and $FeCl_3$ were used as the sources of iron ions to initiate the homogeneous Fenton reaction, in which it was possible to test the dissolved iron ions in the Fe_3S_4 photo-Fenton systems could induce H_2O_2 conversion to ·OH for the SMX degradation. As shown in Fig. S3, SMX could be degraded slightly under the homogeneous Fenton reaction, which excluded the major contribution of homogeneous Fenton reaction to the SMX degradation in the Fe_3S_4 Fenton systems. By comparing the PXRD patterns of Fe_3S_4 before and after photo-Fenton reaction (Fig. 4c), it was revealed that minor S^0 and FeOOH appeared on the used Fe_3S_4 (Shi et al., 2020) and the chemical constitution of the Fe_3S_4 still kept unchanged even after ten cycles.

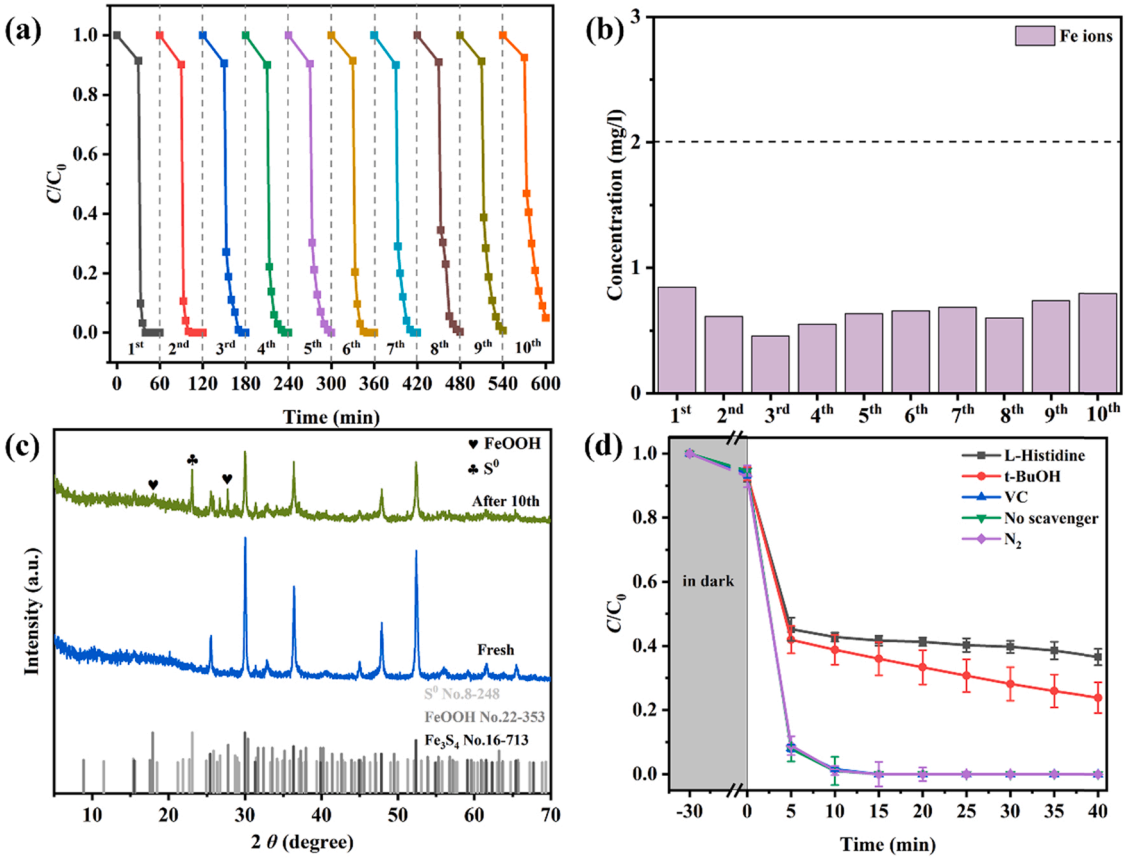

Fig. 4. (a) Cycle use of Fe_3S_4 as photo-Fenton catalysts in the SMX degradation under visible light irradiation. (b) The concentrations of the leached Fe ions during the reusability tests. (c) XRD patterns of the Fe_3S_4 before and after the cyclic experiments. (d) Active species capture results of photo-Fenton SMX degradation over Fe_3S_4 under visible light irradiation. Reaction conditions: Fe_3S_4 dosage = 0.3 g/L, SMX concentration = 5 mg/L, initial pH = 5 (unadjusted), H_2O_2 concentration = 200 μL/L.

The photo-Fenton degradation process of SMX, SIM and SDZ in their mixed solution using the Fe_3S_4 Fenton system was explored. It was observed that the degradation efficiency toward the three mixed sulfonamide solutions reached 100% within 20 min. The observed degradation reaction rates of the three sulfonamides followed a decreasing order of SDZ > SMX > SIM (Fig. S4). Furthermore, the TOC removal efficiencies toward SMX, SIM and SDZ over Fe_3S_4 in the photo-Fenton system was 45.9%,43.6% and 38.1% within 40.0 min under the visible light. The results indicate that Fe_3S_4 can serve as promising materials for the real wastewater treatment. It was well known that Fe_3S_4 can be prepared via different approaches (Table S2), in which Zhang and coworker adopted the Fe_3S_4 as photo-Fenton catalyst to accomplish complete atrazine (15 mg/L) degradation within 35 min under the visible light (Shi et al., 2020). The identical experiment described by Zhang and coworker was conducted, in which the as-prepared Fe_3S_4 from MIL-100(Fe) in our work was used as catalyst. The result revealed that complete atrazine (15 mg/L) degradation can be achieved within 10 min under the visible light (Table S3 and Fig. S5), indicating that the Fe_3S_4 derived from MIL-100(Fe) in our work displayed superior photo-Fenton activity to toward organics degradation.

3.2.5. *The possible degradation mechanisms*

To understand the mechanism of the synergistic effect in the Fe_3S_4/H_2O_2/vis system, the current response density and electron transfer ability of Fe_3S_4 and the precursor MIL-100(Fe) in visible light were investigated. The results revealed that Fe_3S_4 can be excited to produce light-induced electron by the light with wide spectrum. It can be seen that the charge transfer resistance of Fe_3S_4 in Fig. S6 was smaller under visible light, indicated the greatly facilitated separation and transfer of photo-generated electrons (Cao et al., 2020; Zhang et al., 2020).

Series ROS capture experiments were performed to identify the reactive radical species involved in the process and to investigate the heterogeneous photo-Fenton mechanism over Fe_3S_4 as catalyst. The tertiary butyl alcohol (t-BuOH) and L-histidine were selected as ROSs scavengers to quench the radicals of ·OH and $^1O_2$ (Zhou et al., 2020). Also, ascorbic acid was selected to capture $\cdot O_2^-$ and bubbling N_2 eliminated O_2 involvement in the photo-Fenton reaction (Fig. 4d). As to the Fe_3S_4 Fenton system, the introduction of tertiary butyl alcohol significantly could reduce the SMX degradation efficiency, indicating that the main ROS corresponding to the SMX degradation is ·OH radicals. As well, another major ROS contributed to the SMX degradation is non-radical $^1O_2$, due to that the appearance of L-histidine significantly reduces the degradation efficiency of SMX. In contrast, little decrease in the degradation efficiency was observed in the presence of the $\cdot O_2^-$ scavengers ascorbic acid and bubbling N_2 gas, suggesting that $\cdot O_2^-$ did not play a primary role in this photo-Fenton system (He et al., 2021).

To further elucidate the possible mechanism, ESR measurements were carried out to determine the formation of reactive species on Fe_3S_4 during the photo-Fenton process (Fig. 5a–c). Under visible light illumination, characteristic ESR signals of ·OH, $\cdot O_2^-$ and $^1O_2$ are observed over Fe_3S_4, where the peak intensities of ·OH, $\cdot O_2^-$ and $^1O_2$ at 10 min lighting are stronger than those at 5 min, demonstrating that ·OH, $\cdot O_2^-$ and $^1O_2$ were consistently formed in the presence of suitable light, H_2O_2 and Fe_3S_4 catalyst.

The presence of ·OH radicals has been studied by a fluorescence method (Sharma and Feng, 2019). The ·OH can be selectively trapped by terephthalic acid to produce the fluorescent product 2-hydroxy terephthalic acid, which can be excited at 315 nm and fluoresces at 425 nm.

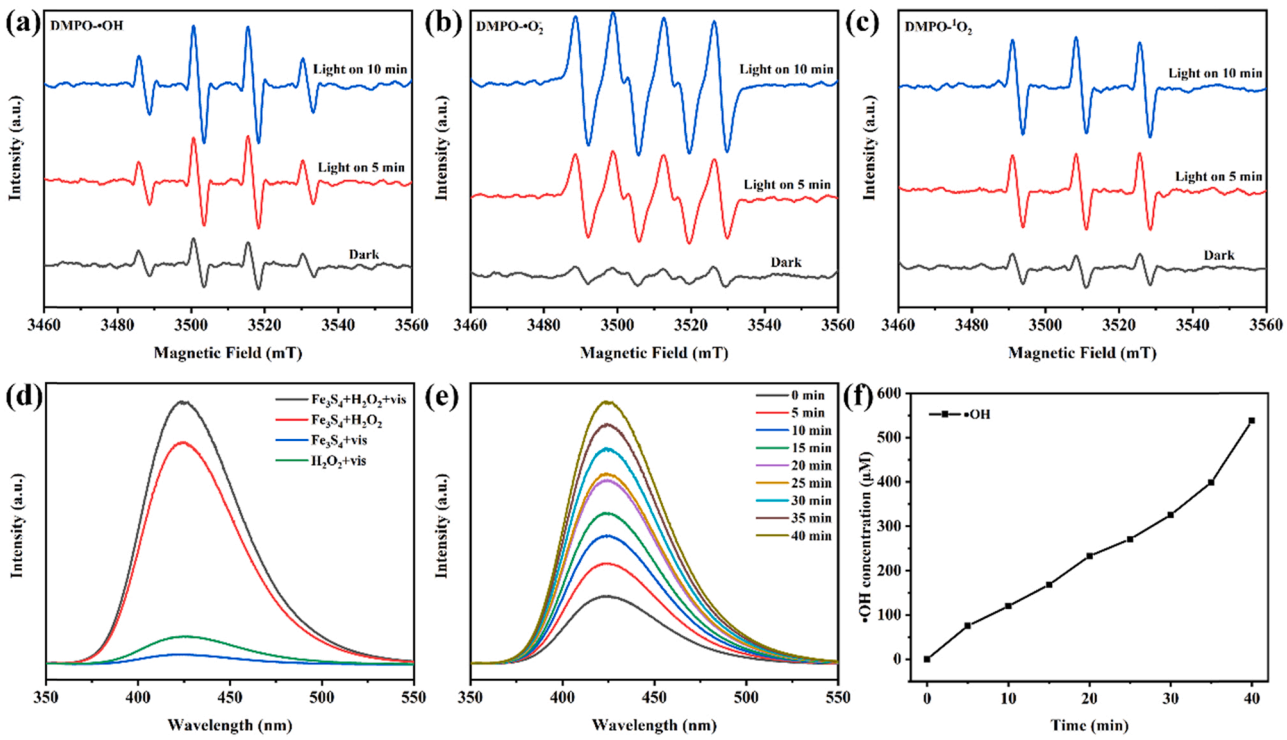

Fig. 5. ESR spectra detected in Fenton systems for (a) DMPO-·OH, (b) DMPO-·O_2^- and (c) DMPO-$^1O_2$. Fluorescence emission spectra of ·OH radicals generated: (d) Different systems and (e) times. (f) Accumulative ·OH production in the Fe_3S_4 Fenton systems. Reaction conditions: Fe_3S_4 dosage = 0.3 g/L, SMX concentration = 5 mg/L, initial pH = 5 (unadjusted), H_2O_2 concentration = 200 μL/L, light source: visible light.

Also, the concentration of ·OH radicals is proportional to the intensity of the peak at 426 nm (Fu et al., 2020; Sharma and Feng, 2019). The fluorescent probe experiment results were similar to the photo-Fenton procedure, except that a solution of 2 mM NaOH and 0.5 mM terephthalic acid was used instead of the original solution containing SMX. As shown in Fig. 5d, no obvious fluorescence intensity was observed within individual Fe_3S_4 and visible light, respectively, suggesting that few ·OH radicals were yielded. In the Fe_3S_4/H_2O_2 system, the fluorescence intensity gradually increased at 425 nm can be detected, demonstrating that the simultaneous presence of H_2O_2 and Fe_3S_4 can lead to significant yield of ·OH radicals via Eqs. (1) and (2). The strongest fluorescence intensity in the H_2O_2/Fe_3S_4/visible light system demonstrated that more ·OH radicals can be generated, in which the intensity of the fluorescence increased linearly with the reaction time (Fig. 5e). This confirms that the production of ·OH during the photo-Fenton process is the key active species for oxidative SMX degradation. As expected, the removal of SMX was highly reliant on the generation of ·OH radicals. It was calculated that 537 μmol/L of ·OH radicals can be yielded in the H_2O_2/Fe_3S_4/visible light system within 40.0 min (Fig. 5f).

$$Fe^{3+} + H_2O_2 \rightarrow Fe^{2+} + \cdot HOO + H^+ \quad (1)$$

$$Fe^{2+} + H_2O_2 \rightarrow Fe^{3+} + \cdot OH + OH^- \quad (2)$$

The XPS spectra of Fe 2p, S 2p and O 1s before and after SMX degradation were also analyzed. The peak at 706.9 eV in the HR-XPS spectrum of fresh Fe_3S_4 could be ascribed to the presence of Fe(II)-S species (Fig. S7b). All the peaks at 708.1, 710.0, 711.1 and 712.1 eV could be contributed to the formation of Fe(III)-S species (Liu et al., 2019; Shi et al., 2020). Peak splits of O 1s (Fig. S7d) at 529.9, 531.5 and 532.3 eV were ascribed to O_2^-, OH^- and H_2O, respectively. The peak at 713.4 eV is attributed to the Fe(III)-O species, which is the result of the oxidation of Fe_3S_4 surface, which was further confirmed by the HR-XPS spectra of O1s. The decrease in Fe(II)-S species and the increase in Fe (III)-O species on the recycled Fe_3S_4 surface demonstrated the high oxidation capacity of Fe(II) to SMX removal and the conversion of ferrous species to Fe(III)-O species on the Fe_3S_4 surface. After 10 cycles, the S_{bulk}^{2-} (162.4 eV) and $S_{surface}^{2-}$ (161.2 eV) species of Fe_3S_4 decreased, which was inferred to be oxidized into S^0 (164.9 eV). These trends pointed that the Fe_3S_4 surface would produce FeOOH and S^0 in- situ, inhibiting the internal Fe(II)-S species reaction with H_2O_2 and ultimately resulting in lower ·OH yields. Nevertheless, visible light illumination could promote the conversion of more H_2O_2 to ·OH, completing the removal of SMX. In addition, comparing with the fresh Fe_3S_4, the binding energies of Fe(III)-S and Fe(II)-S species in the reacted Fe_3S_4 were clearly transformed to higher or lower values. These variations were induced by chemical interaction between SMX and Fe_3S_4 (Yang et al., 2020).

Based on the previous analysis, a probable Fe(II)/Fe(III) cycle mechanism for the Fe_3S_4 photo-Fenton system in the degradation of SAs was proposed (Scheme 2). The Fe^{2+} could be released from Fe_3S_4, which could then react with H_2O_2 to generate ·OH, accompanying with the production of Fe^{3+} (Eq. (2)). These ·OH may directly oxidize SAs while the generated Fe^{3+} could produce FeOOH complexes over the surface of Fe_3S_4, which disfavored the further photo-Fenton reaction (Wang et al., 2020). Fortunately, the surficial Fe^{2+} on the Fe_3S_4 could activate the molecular oxygen (O_2) to produce non-radical ·O_2^- via the single-electron transfer pathway (Eq. (3)), which might reduce the surficial Fe^{3+} into Fe^{2+} (Eq. (4)). These abundant ·O_2^- were further transformed into ·OH and $^1O_2$ (Eqs. (5) and (6)). The abundance of both photo-produced electrons and ·O_2^- over the visible light responsive Fe_3S_4 ensures the effective regeneration and recyclability of iron species in Fe_3S_4. The effectual Fe(II)/Fe(III) cycle in the Fe_3S_4/H_2O_2/light system could offer surficial Fe^{2+} for the process to produce more ·OH and $^1O_2$ for enhancing the SAs degradation efficiencies (Eq. (7)).

$$Fe^{2+} + O_2 \rightarrow Fe^{3+} + \cdot O_2^- \quad (3)$$

$$Fe^{3+} + \cdot O_2^- \rightarrow Fe^{2+} + O_2 \quad (4)$$

$$2 \cdot O_2^- + 2H^+ \rightarrow {}^1O_2 + H_2O_2 \quad (5)$$

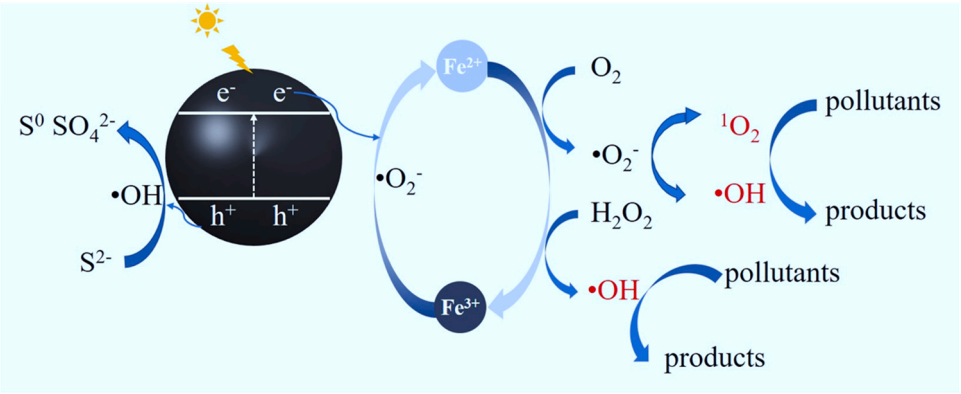

Scheme 2. Mechanistic scheme of photo-Fenton reaction over Fe_3S_4 for SMX degradation.

$$2{\cdot}O_2^- + 2H^+ \rightarrow 2{\cdot}OH + O_2 \quad (6)$$

$$\cdot OH/^1O_2 + \text{pollutants} \rightarrow \text{degraded products} \quad (7)$$

3.2.6. The influence of co-existing inorganic anions on SMX degradation

The co-existing inorganic anions in the real water environment can significantly influence the catalytic AOPs degradation activity toward organic pollutants (Yi et al., 2021). To further clarify the potential of the photo-Fenton system for practical applications, the effect of co-existing inorganic anions like Cl^-, NO_3^-, SO_4^{2-}, HCO_3^- and $H_2PO_4^-$ in surface water on the catalytic degradation toward SMX were investigated. The parameters of water quality are shown in the Table S4, which were simulated from the water quality standard of surface water in Beijing. As shown in Fig. 6a, the Cl^-, NO_3^- and SO_4^{2-} anions exerted negligible effect on SMX degradation activity. However, the degradation efficiencies maintained well after the introduction of $H_2PO_4^-$ anions to the degradation system, due to that the $H_2PO_4^-$ anion concentration in the real surface water is low. With the increasing concentration of HCO_3^- up to 272.0 mg/L, the SMX degradation ability of Fe_3S_4 was significantly inhibited. The HCO_3^- anions not only act as buffer mediate (Jiang et al., 2020), but also as ·OH scavenger, which can transform the highly active ·OH radicals to weakly oxidative species (Zhao et al., 2021). When

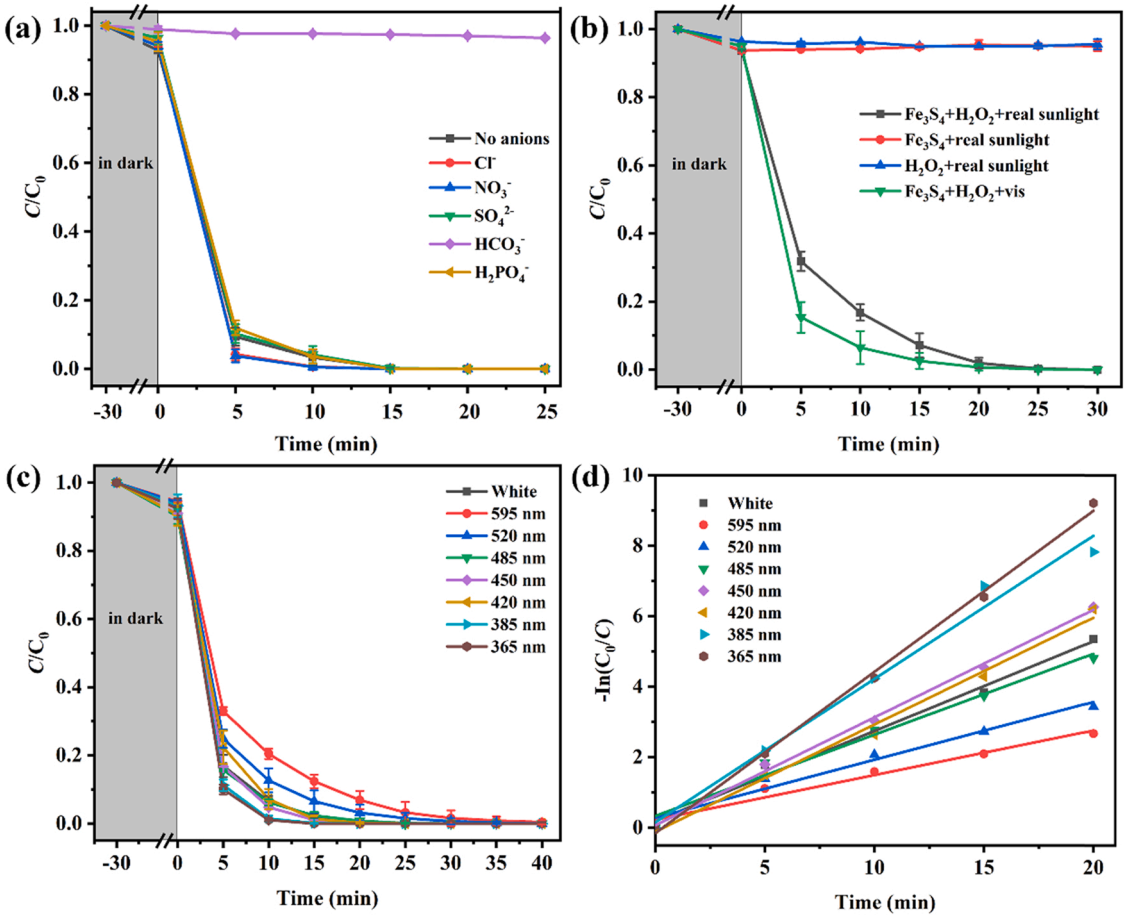

Fig. 6. (a) Effect of inorganic anions on the SMX degradation under visible light irradiation. (b) Photodegradation of SMX under different light sources. (c) Effect of SMX degradation under lights with different wavelengths. (d) The *k* values of SMX degradation under lights with different wavelengths. Reaction conditions: Fe_3S_4 dosage = 0.3 g/L, SMX concentration = 5 mg/L, initial pH = 5 (unadjusted), H_2O_2 concentration = 200 μL/L.

HCO_3^- was added into the SMX solution, the pH of the solution changed from 5.0 to 7.7. From these points, the significant reduction of the SMX degradation efficiencies of Fe_3S_4/H_2O_2/visible light system could be contributed to that HCO_3^- might markedly increase the solution pH and markedly consume the formed ·OH radicals.

3.2.7. *Effect of different light sources*

Field experiments of SMX degradation of over different systems were carried out under real solar illumination conditions using Fe_3S_4 as a catalyst. The real solar spectra are shown in Fig. S8. In Fig. 6b, SMX could be hardly degraded in the absence of either catalyst or H_2O_2. In contract, the system of Fe_3S_4/real sunlight/H_2O_2 achieved 100% SMX degradation efficiency within 25 min under the real sunlight (25 mW), which was slightly lower than the oxidation efficiency under the visible light illumination (320 mW) in lab. Considering the abundant availability of sunlight, the SMX degradation in the Fe_3S_4/real sunlight/H_2O_2 system demonstrated potentially practical application.

To investigate the effect of different light source on the SMX degradation efficiency over Fe_3S_4 with the presence of H_2O_2, a series of experiments were carried out under the monochromatic light with the wavelength of 365 nm, 385 nm, 420 nm, 450 nm, 485 nm, 520 nm, 595 nm and white light. The PCX50B Discover multichannel photochemical reaction system (Beijing Perfectlight Technology Co., Ltm) with was adopted to supply all different lights with the optical power being 162.5 mW (UV365),188.0 mW (UV385), 175.8 mW (purple), 156.7 mW (blue), 104.9 mW (cyan), 103.5 mW (green), 36.5 mW (orange) and 198.1 mW (white), respectively. It was interesting to find that within 40 min, SMX can be completely degraded via photo-Fenton-like reaction in different light source with the aid the Fe_3S_4 and H_2O_2 (Fig. 6c). The kinetic plots of SMX decomposition in above-mentioned systems were fitted well with the pseudo-first-order model (Fig. 6d). The SMX photo-Fenton degradation reactions were strongly dependent on the irradiation wavelength of the light source, which can be attributed to the energy of the photon depends on the wavelength (Chen et al., 2019). It was observed that better photo-Fenton performance was found under UV light than under visible light, which also corroborates with the

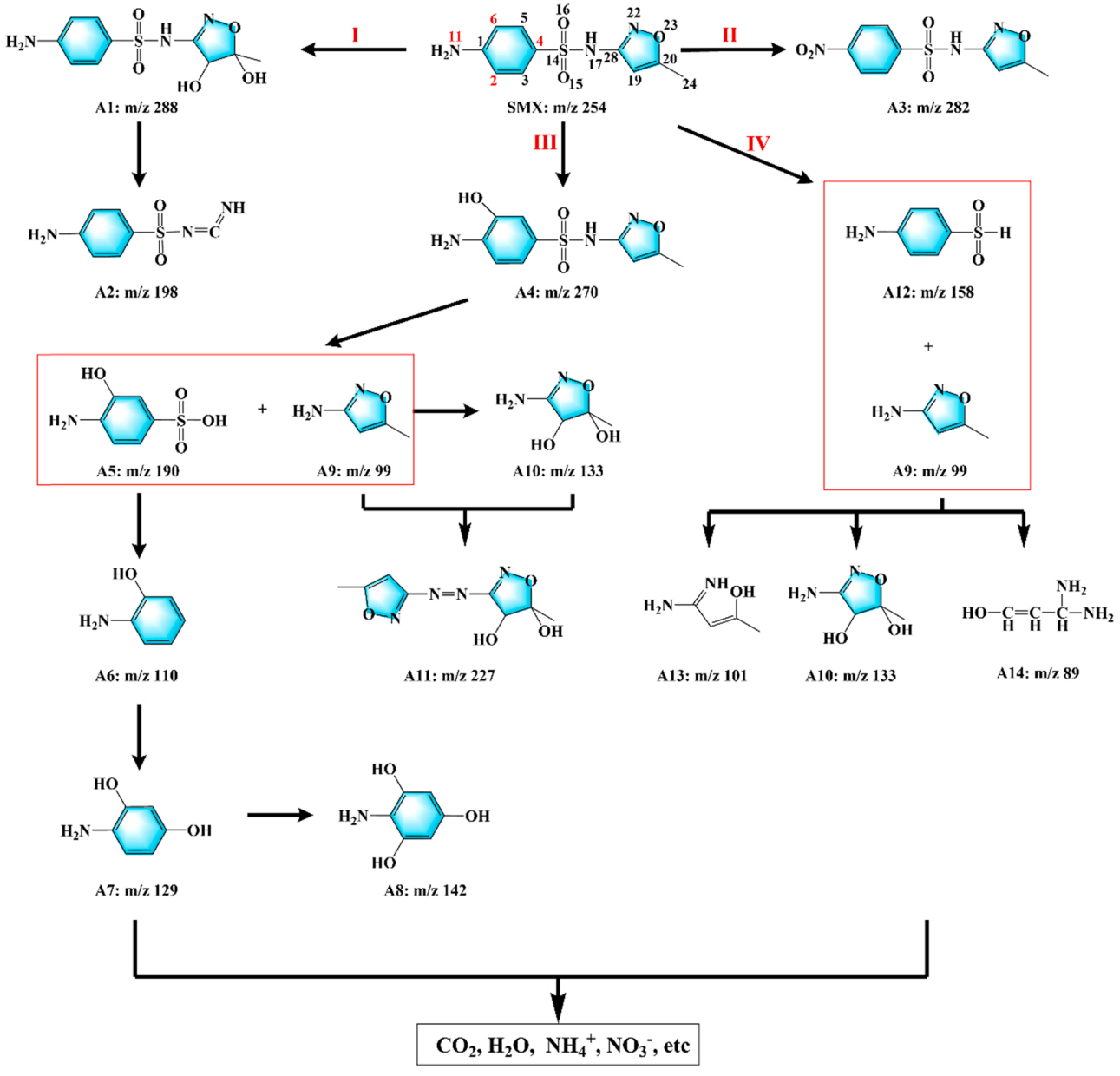

Fig. 7. Proposed SMX degradation pathway over Fe_3S_4/H_2O_2/Vis system.

results in Fig. 3a. There was little difference in the photo-Fenton degradation rate of SMX under different wavelengths of light irradiation, which is consistent with the UV–Vis/DRS results (Fig. S1). These results demonstrates that Fe_3S_4 has great potential for practical applications under different light sources.

3.2.8. The SAs degradation pathway in the photo-Fenton system over Fe_3S_4

The Fukui function based on the DFT calculation by Liu's group was adopted to further explore the relationship between radicals attacking and the intermediates of SMX molecules (Peng et al., 2021). Liu's group reported that the C2 ($f^- = 0.1617$), C4 ($f^- = 0.1934$), C6 ($f^- = 0.1470$) and N11 ($f^- = 0.2942$) in the SMX molecule are the active sites with higher electrophilic attack Fukui values, which are proved to be attacked by both ·OH radicals and $^1O_2$ non-radicals. The SMX degradation pathway was proposed via the determination of the intermediate products formed in the process of SMX degradation obtained UPLC-MS.

In pathway I (Fig. 7), both the electrophilic addition and electrophilic substitution of ·OH to the C═C bond of the isoxazole ring resulted into the formation of A1 as dihydroxylated SMX (Du et al., 2018a). In pathway II, N11 of SMX with the highest f^- value can also be oxidized to form A3, which is the classical oxidative product of SMX. Pathway III was regarded as the major decomposition pathway of SMX attacked by ·OH radicals, in which the electrophilic substitution of ·OH occurring on the aromatic ring led to the formation of the ortho-hydroxylated SMX (A4). Also, the ·OH radicals participated into attacking the S—N bond of A4 to produce A5 and A9. The ongoing electrophilic substitution of ·OH might form A8. The generation of A11 was the shared pathway through coupling of the N-centered radical derived from $–NH_2$ group of A9 and A10. Pathway Ⅳ was the sulfonamide bond cleavage, the products included A12 and A9. A9 was oxidized to A13, A14 and A15, whereas products were transformed into single-chain compounds through a series of oxidation reactions, until final degradation occurred (Li et al., 2021).

As to SIM, in pathway I (Fig. S9), the reaction of ·OH radicals to attack SIM was the generation of hydroxylated products (Ge et al., 2019). This is followed by a substitution reaction to produce B2. In pathway II, the oxidative ring opening of the isoxazole ring formed B3 (Wang et al., 2016). The third degradation pathway was via the isoxazole ring substitution reaction of SIM to produce the intermediate at B4. Later, the isoxazole ring could be oxidized to form B7 via opening the isoxazole ring. In pathway Ⅳ, the S-N bond in the sulfadiazine molecule was attacked by ·OH radicals to produce the B8 and B13 as intermediates, which could further be transformed to B9 after a series of oxidation and substitution reactions (Wang et al., 2021). At the same time, the S-C bond in B9 is attacked by ·OH and cleaved into B10 and B11.

Also, Deng's group (Duan et al., 2020) showed that N1, N4, C5, C6, O2 and O3 atoms in SDZ holding larger f^0 are more vulnerable to the radicals attack. Based on the detected intermediates and Fukui index, the degradation pathway of SDZ is schematically proposed in Fig. S10. Firstly, the C–N bond in the pyrimidine ring could be attacked by ·OH radicals to form intermediate D1 with the evidence of the oxidation of $–NH_2$ into $–NO_2$ (Yang et al., 2018). In pathway II, the sulfadiazine readily loses electrons at the N position, resulting into the break of the H-N bond to produce the sulfadiazine radicals. The above-mentioned reactive radicals underwent the coupling reactions to form D3. The S-N bond of the D3 could be attacked by ·OH to yield intermediate D4. Pathway III was formed via the break of S–N bond by ·OH radical, and D6 and D8 were generated. By the continuous attacking of ·OH to D6, D7 was produced. Meanwhile, D12 was formed by the oxidation of D8 by ·OH while the formation of D9 between D6 and D8 was also a common reaction in SDZ degradation by ·OH (Yang and Che, 2017). In pathway Ⅳ, sulfadiazine could also hydroxylate to produce D13 (Chen et al., 2021). The intermediate D15 was produced by the C-N bond cleavage in the pyrimidine ring. The D15 was attacked by ·OH cleaving the potential site of S-N bond and also hydroxylation, forming D16. There were two possible products (D17 and D18) emerging from D16. Further, D19 was also generated by the extrusion of SO_2 from D17. D19 was possible intermediates generating from D18 (Yadav et al., 2018).

4. Conclusion

In summary, we facilely derived Fe_3S_4 using classical MIL-100(Fe) as a precursor, which exhibited better performance than the directly synthesized Fe_3S_4 for the photo-Fenton degradation of SAs under both UV and visible light. The effects of different systems, initial pH, catalyst dosage, H_2O_2 concentration, real water, foreign ions, real sunlight and different monochrome lights on the photocatalytic performance were elucidated. Furthermore, cycling experiments for SMX degradation showed that the derived Fe_3S_4 was stable and favorable for recovery by magnetism. In addition, the degradation pathways assessments of SMX, SIM, SDZ during the photo-Fenton process were also presented and tested. The efficient degradation of SAs by the Fe_3S_4 Fenton system was attributed to the acceleration of Fe(II)/Fe(III) cycling on the Fe_3S_4 surface by photogenerated electrons and $\cdot O_2^-$, which favored the decomposition of H_2O_2 to produce more. The present work shows that some metal sulfides with special morphologies and enhanced photocatalytic properties can be prepared by tunable MOFs. These interesting findings could provide some new insights into the heterogeneous photo-Fenton of derivative biodegradation of organic pollutants in the environment.

CRediT authorship contribution statement

Jing Hang: Data curation, Investigation, Visualization, Writing – original draft. **Xiao-Hong Yi:** Methodology, Software. **Chong-Chen Wang:** Conceptualization, Funding acquisition, Supervision, Project administration, Writing – review & editing. **Huifen Fu:** Conceptualization, Funding acquisition, Supervision, Project administration, Methodology. **Peng Wang:** Resources, Instrumental. **Yijiang Zhao:** Methodology, Software.

Declaration of Competing Interest

The authors declare that they have no known competing financial interests or personal relationships that could have appeared to influence the work reported in this paper.

Acknowledgements

This work was supported by National Natural Science Foundation of China (22176012, 51878023, 21806008), Beijing Natural Science Foundation (8202016), Great Wall Scholars Training Program Project of Beijing Municipality Universities (CIT&TCD20180323), Beijing Talent Project (2020A27), Science and Technology General Project of Beijing Municipal Education Commission (KM202110016010). The Fundamental Research Funds for Beijing University of Civil Engineering and Architecture (X20147/X20141/X20135/X20146) and the BUCEA Post Graduate Innovation Project (PG2021048).

Appendix A. Supporting information

Supplementary data associated with this article can be found in the online version at doi:10.1016/j.jhazmat.2021.127415.

References

Ahmad, M., Chen, S., Ye, F., Quan, X., Afzal, S., Yu, H., Zhao, X., 2019. Efficient photo-Fenton activity in mesoporous MIL-100(Fe) decorated with ZnO nanosphere for pollutants degradation. Appl. Catal. B: Environ. 245, 428–438.

Ai, L., Zhang, C., Li, L., Jiang, J., 2014. Iron terephthalate metal–organic framework: revealing the effective activation of hydrogen peroxide for the degradation of organic dye under visible light irradiation. Appl. Catal. B: Environ. 148–149, 191–200.

Campbell, M.G., Dincă, M., 2017. Metal–organic frameworks as active materials in electronic sensor devices. Sensors 17, 1108.
Cao, P., Quan, X., Zhao, K., Chen, S., Yu, H., Niu, J., 2020. Selective electrochemical H_2O_2 generation and activation on a bifunctional catalyst for heterogeneous electro-Fenton catalysis. J. Hazard. Mater. 382, 121102.
Carra, I., Malato, S., Jiménez, M., Maldonado, M.I., Sánchez Pérez, J.A., 2014. Microcontaminant removal by solar photo-Fenton at natural pH run with sequential and continuous iron additions. Chem. Eng. J. 235, 132–140.
Chen, Q., Chen, L., Qi, J., Tong, Y., Lv, Y., Xu, C., Ni, J., Liu, W., 2019. Photocatalytic degradation of amoxicillin by carbon quantum dots modified $K_2Ti_6O_{13}$ nanotubes: effect of light wavelength. Chin. Chem. Lett. 30, 1214–1218.
Chen, X., Oh, W.-D., Hu, Z.-T., Sun, Y.-M., Webster, R.D., Li, S.-Z., Lim, T.-T., 2018. Enhancing sulfacetamide degradation by peroxymonosulfate activation with N-doped graphene produced through delicately-controlled nitrogen functionalization via tweaking thermal annealing processes. Appl. Catal. B: Environ. 225, 243–257.
Chen, X., Deng, F., Liu, X., Cui, K.-P., Weerasooriya, R., 2021. Hydrothermal synthesis of MnO_2/Fe(0) composites from Li-ion battery cathodes for destructing sulfadiazine by photo-fenton process. Sci. Total Environ. 774, 145776.
Clarizia, L., Russo, D., Di Somma, I., Marotta, R., Andreozzi, R., 2017. Homogeneous photo-Fenton processes at near neutral pH: a review. Appl. Catal. B: Environ. 209, 358–371.
Daud, N.K., Hameed, B.H., 2010. Decolorization of Acid Red 1 by Fenton-like process using rice husk ash-based catalyst. J. Hazard. Mater. 176, 938–944.
Deng, Y., Xing, M., Zhang, J., 2017. An advanced $TiO_2/Fe_2TiO_5/Fe_2O_3$ triple-heterojunction with enhanced and stable visible-light-driven fenton reaction for the removal of organic pollutants. Appl. Catal. B: Environ. 211, 157–166.
Du, J., Guo, W., Che, D., Ren, N., 2018a. Weak magnetic field for enhanced oxidation of sulfamethoxazole by Fe^0/H_2O_2 and Fe^0/persulfate: performance, mechanisms, and degradation pathways. Chem. Eng. J. 351, 532–539.
Du, J., Guo, W., Wang, H., Yin, R., Zheng, H., Feng, X., Che, D., Ren, N., 2018b. Hydroxyl radical dominated degradation of aquatic sulfamethoxazole by Fe^0/bisulfite/O_2: kinetics, mechanisms, and pathways. Water Res. 138, 323–332.
Duan, Y., Deng, L., Shi, Z., Liu, X., Zeng, H., Zhang, H., Crittenden, J., 2020. Efficient sulfadiazine degradation via in-situ epitaxial grow of Graphitic Carbon Nitride (g-C_3N_4) on carbon dots heterostructures under visible light irradiation: synthesis, mechanisms and toxicity evaluation. J. Colloid Interface Sci. 561, 696–707.
Fang, Y., Yang, Z., Li, H., Liu, X., 2020. MIL-100(Fe) and its derivatives: from synthesis to application for wastewater decontamination. Environ. Sci. Pollut. Res. 27, 4703–4724.
Fu, H., Song, X.-X., Wu, L., Zhao, C., Wang, P., Wang, C.-C., 2020. Room-temperature preparation of MIL-88A as a heterogeneous photo-Fenton catalyst for degradation of rhodamine B and bisphenol a under visible light. Mater. Res. Bull. 125, 110806.
Ge, L., Zhang, P., Halsall, C., Li, Y., Chen, C.-E., Li, J., Sun, H., Yao, Z., 2019. The importance of reactive oxygen species on the aqueous phototransformation of sulfonamide antibiotics: kinetics, pathways, and comparisons with direct photolysis. Water Res. 149, 243–250.
Guo, T., Wang, K., Zhang, G., Wu, X., 2018. A novel α-Fe_2O_3@g-C_3N_4 catalyst: synthesis derived from Fe-based MOF and its superior photo-Fenton performance. Appl. Surf. Sci. 469, 331–339.
He, W., Li, Z., Lv, S., Niu, M., Zhou, W., Li, J., Lu, R., Gao, H., Pan, C., Zhang, S., 2021. Facile synthesis of Fe_3O_4@MIL-100(Fe) towards enhancing photo-Fenton like degradation of levofloxacin via a synergistic effect between Fe_3O_4 and MIL-100(Fe). Chem. Eng. J. 409, 128274.
Jiang, D., Chen, M., Wang, H., Zeng, G., Huang, D., Cheng, M., Liu, Y., Xue, W., Wang, Z., 2019. The application of different typological and structural MOFs-based materials for the dyes adsorption. Coord. Chem. Rev. 380, 471–483.
Jiang, J., Wang, X., Liu, Y., Ma, Y., Li, T., Lin, Y., Xie, T., Dong, S., 2020. Photo-Fenton degradation of emerging pollutants over Fe-POM nanoparticle/porous and ultrathin g-C_3N_4 nanosheet with rich nitrogen defect: degradation mechanism, pathways, and products toxicity assessment. Appl. Catal. B: Environ. 278, 119349.
Jiao, L., Wang, Y., Jiang, H.-L., Xu, Q., 2018. Metal–organic frameworks as platforms for catalytic applications. Adv. Mater. 30, 1703663.
Kallel, M., Belaid, C., Mechichi, T., Ksibi, M., Elleuch, B., 2009. Removal of organic load and phenolic compounds from olive mill wastewater by Fenton oxidation with zero-valent iron. Chem. Eng. J. 150, 391–395.
Li, Q., Wei, Q., Zuo, W., Huang, L., Luo, W., An, Q., Pelenovich, V.O., Mai, L., Zhang, Q., 2017. Greigite Fe_3S_4 as a new anode material for high-performance sodium-ion batteries. Chem. Sci. 8, 160–164.
Li, R., Zhang, W., Zhou, K., 2018. Metal–organic-framework-based catalysts for photoreduction of CO_2. Adv. Mater. 30, 1705512.
Li, T., Ge, L., Peng, X., Wang, W., Zhang, W., 2021. Enhanced degradation of sulfamethoxazole by a novel Fenton-like system with significantly reduced consumption of H_2O_2 activated by g-C_3N_4/MgO composite. Water Res. 190, 116777.
Li, Y.-H., Yi, X.-H., Li, Y.-X., Wang, C.-C., Wang, P., Zhao, C., Zheng, W., 2021. Robust Cr (VI) reduction over hydroxyl modified UiO-66 photocatalyst constructed from mixed ligands: Performances and mechanism insight with or without tartaric acid. Environ. Res. 201, 111596.
Li, Y.-X., Han, Y.-C., Wang, C.-C., 2021a. Fabrication strategies and Cr(VI) elimination activities of the MOF-derivatives and their composites. Chem. Eng. J. 405, 126648.
Li, Y.-X., Wang, C.-C., Fu, H., Wang, P., 2021b. Marigold-flower-like TiO_2/MIL-125 core-shell composite for enhanced photocatalytic Cr(VI) reduction. J. Environ. Chem. Eng. 9 (4), 105451.
Liu, J., Guo, X., Zhao, Z., Li, B., Qin, J., Peng, Z., He, G., Brett, D.J.L., Wang, R., Lu, X., 2020. Fe_3S_4 nanoparticles for arterial inflammation therapy: integration of magnetic hyperthermia and photothermal treatment. Appl. Mater. Today 18, 100457.
Liu, W., Ai, Z., Dahlgren, R.A., Zhang, L., Wang, X., 2017. Adsorption and reduction of roxarsone on magnetic greigite (Fe_3S_4): indispensable role of structural sulfide. Chem. Eng. J. 330, 1232–1239.
Liu, W., Jin, L., Xu, J., Liu, J., Li, Y., Zhou, P., Wang, C., Dahlgren, R.A., Wang, X., 2019. Advanced MaterialsInsight into pH dependent Cr(VI) removal with magnetic Fe_3S_4. Chem. Eng. J. 359, 564–571.
Luo, H., Zhuotong, Z., Zeng, G., Zhang, C., Xiao, R., Huang, D., Lai, C., Cheng, M., Wang, W., Xiong, W., Yang, Y., Qin, L., Zhou, C., Han, W., Zhou, Y., Tian, S., 2019. Recent progress on metal-organic frameworks based- and derived- photocatalysts for water splitting. Chem. Eng. J. 383, 123196.
Luo, J., Hu, Y., Xiao, L., Zhang, G., Guo, H., Hao, G., Jiang, W., 2019. Synthesis of 3D flower-like Fe3S4 microspheres and quasi-sphere Fe3S4-RGO hybrid-architectures with enhanced electromagnetic wave absorption. Nanotechnology 31, 085708.
Peng, J., Zhou, P., Zhou, H., Liu, W., Zhang, H., Zhou, C., Lai, L., Ao, Z., Su, S., Lai, B., 2021. Insights into the electron-transfer mechanism of permanganate activation by graphite for enhanced oxidation of sulfamethoxazole. Environ. Sci. Technol. 55, 9189–9198.
Ramirez, J.H., Maldonado-Hódar, F.J., Pérez-Cadenas, A.F., Moreno-Castilla, C., Costa, C.A., Madeira, L.M., 2007. Azo-dye Orange II degradation by heterogeneous Fenton-like reaction using carbon-Fe catalysts. Appl. Catal. B: Environ. 75, 312–323.
Roberts, A.P., Reynolds, R.L., Verosub, K.L., Adam, D.P., 1996. Environmental magnetic implications of Greigite (Fe_3S_4) Formation in a 3 m.y. lake sediment record from Butte Valley, northern California. Geophys. Res. Lett. 23, 2859–2862.
Roldan, A., Leeuw, N., 2015. Methanol formation from CO_2 catalyzed by Fe_3S_4{111}: formate versus hydrocarboxyl pathways. Faraday Discuss. 188, 161–180.
Sharma, V.K., Feng, M., 2019. Water depollution using metal-organic frameworks-catalyzed advanced oxidation processes: a review. J. Hazard. Mater. 372, 3–16.
Shi, W., Du, D., Shen, B., Cui, C., Lu, L., Wang, L., Zhang, J., 2016. Synthesis of yolk–shell structured Fe_3O_4@void@CdS nanoparticles: a general and effective structure design for photo-fenton reaction. ACS Appl. Mater. Interfaces 8, 20831–20838.
Shi, Y., Wang, X., Liu, X., Ling, C., Shen, W., Zhang, L., 2020. Visible light promoted Fe_3S_4 fenton oxidation of atrazine. Appl. Catal. B: Environ. 277, 119229.
Villegas- Guzman, P., Giannakis, S., Rtimi, S., Grandjean, D., Bensimon, M., de Alencastro, L.F., Torres-Palma, R., Pulgarin, C., 2017. A green solar photo-Fenton process for the elimination of bacteria and micropollutants in municipal wastewater treatment using mineral iron and natural organic acids. Appl. Catal. B: Environ. 219, 538–549.
Wang, F., Fu, H., Wang, F.-X., Zhang, X.-W., Wang, P., Zhao, C., Wang, C.-C., 2022. Enhanced catalytic sulfamethoxazole degradation via peroxymonosulfate activation over amorphous CoSx@SiO2 nanocages derived from ZIF-67. J. Hazard. Mater. 423, 126998.
Wang, J.-W., Qiu, F.-G., Wang, P., Ge, C., Wang, C.-C., 2021. Boosted bisphenol A and Cr (VI) cleanup over Z-scheme WO_3/MIL-100(Fe) composites under visible light. J. Clean. Prod. 279, 123408.
Wang, W., Tian, J., Zhu, Z., Zhu, C., Liu, B., Hu, C., 2021. Insight into quinolones and sulfonamides degradation, intermediate product identification and decomposition pathways with the assistance of Bi_2MoO_6/Bi_2WO_6/MWCNTs photocatalyst. Process Saf. Environ. 147, 527–546.
Wang, X., Pu, X., Yuan, Y., Xiang, Y., Zhang, Y., Xiong, Z., Yao, G., Lai, B., 2020. An old story with new insight into the structural transformation and radical production of micron-scale zero-valent iron on successive reactivities. Chin. Chem. Lett. 31, 2634–2640.
Wang, Y., Liu, S., Li, R., Huang, Y., Chen, C., 2016. Electro-catalytic degradation of sulfisoxazole by using graphene anode. J. Environ. Sci. 43, 54–60.
Wu, H., Liu, J., Liang, H., Zang, D., 2020. Sandwich-like Fe_3O_4/Fe_3S_4 composites for electromagnetic wave absorption. Chem. Eng. J. 393, 124743.
Wu, X., Zhao, W., Huang, Y., Zhang, G., 2020. A mechanistic study of amorphous CoS_x cages as advanced oxidation catalysts for excellent peroxymonosulfate activation towards antibiotics degradation. Chem. Eng. J. 381, 122768.
Xu, B., Chen, Z., Han, B., Li, C., 2017. Glycol assisted synthesis of MIL-100(Fe) nanospheres for photocatalytic oxidation of benzene to phenol. Catal. Commun. 98, 112–115.
Xu, L., Wang, J., 2011. A heterogeneous Fenton-like system with nanoparticulate zero-valent iron for removal of 4-chloro-3-methyl phenol. J. Hazard. Mater. 186 (1), 256–264.
Yadav, M.S.P., Neghi, N., Kumar, M., Varghese, G.K., 2018. Photocatalytic-oxidation and photo-persulfate-oxidation of sulfadiazine in a laboratory-scale reactor: analysis of catalyst support, oxidant dosage, removal-rate and degradation pathway. J. Environ. Manag. 222, 164–173.
Yang, J.-F., He, M., Wu, T.-F., Hao, A.-P., Zhang, S.-B., Chen, Y.-D., Zhou, S.-B., Zhen, L.-Y., Wang, R., Yuan, Z.-L., Deng, L., 2018. Sulfadiazine oxidation by permanganate: kinetics, mechanistic investigation and toxicity evaluation. Chem. Eng. J. 349, 56–65.
Yang, S., Che, D., 2017. Degradation of aquatic sulfadiazine by Fe0/persulfate: kinetics, mechanisms, and degradation pathway. RSC Adv. 7, 42233–42241.
Yang, S., Zhang, C., Cai, Y., He, X., Niu, H., 2017. Synthesis of $Cd_xZn_{1-x}S$@Fe_3S_4 magnetic photocatalyst nanoparticles for the photodegradation of methylene blue. J. Alloy. Compd. 735, 1955–1961.
Yang, S., Li, Q., Chen, L., Chen, Z., Hu, B., Wang, H., Wang, X., 2020. Synergistic removal and reduction of U(VI) and Cr(VI) by Fe_3S_4 micro-crystal. Chem. Eng. J. 385, 123909.
Yi, X.-H., Ji, H., Wang, C.-C., Li, Y., Li, Y.-H., Zhao, C., Wang, A., Fu, H., Wang, P., Zhao, X., Liu, W., 2021. Photocatalysis-activated SR-AOP over PDINH/MIL-88A(Fe) composites for boosted chloroquine phosphate degradation: performance, mechanism, pathway and DFT calculations. Appl. Catal. B: Environ. 293, 120229.

Zhang, M., Hu, Q., Ma, K., Ding, Y., Li, C., 2020. Pyroelectric effect in CdS nanorods decorated with a molecular Co-catalyst for hydrogen evolution. Nano Energy 73, 104810.

Zhang, X.-W., Wang, F., Wang, C.-C., Wang, P., Fu, H., Zhao, C., 2021. Photocatalysis activation of peroxodisulfate over the supported Fe3O4 catalyst derived from MIL-88A(Fe) for efficient tetracycline hydrochloride degradation. Chem. Eng. J. 426, 131927.

Zhao, C., Wang, J., Chen, X., Wang, Z., Ji, H., Chen, L., Liu, W., Wang, C.-C., 2021. Bifunctional $Bi_{12}O_{17}Cl_2$/MIL-100(Fe) composites toward photocatalytic Cr(VI) sequestration and activation of persulfate for bisphenol A degradation. Sci. Total Environ. 752, 141901.

Zhao, X., Lan, X., Yu, D., Fu, H., Liu, Z., Mu, T., 2018. Deep eutectic-solvothermal synthesis of nanostructured Fe_3S_4 for electrochemical N_2 fixation under ambient conditions. Chem. Commun. 54, 13010–13013.

Zheng, J., Cao, Y., Cheng, C., Chen, C., Yan, R.-W., Huai, H.-X., Dong, Q.-F., Zheng, M.-S., Wang, C.-C., 2014. Facile synthesis of Fe_3S_4 hollow spheres with high-performance for lithium-ion batteries and water treatment. J. Mater. Chem. A 2, 19882–19888.

Zhou, Y., Zhou, L., Zhou, Y., Xing, M., Zhang, J., 2020. Z-scheme photo-Fenton system for efficiency synchronous oxidation of organic contaminants and reduction of metal ions. Appl. Catal. B: Environ. 279, 119365.

Zhou, Z., Li, K., Deng, W., Li, J., Yan, Y., Li, Y., Quan, X., Wang, T., 2020. Nitrogen vacancy mediated exciton dissociation in carbon nitride nanosheets: enhanced hydroxyl radicals generation for efficient photocatalytic degradation of organic pollutants. J. Hazard. Mater. 387, 122023.